Combining Batch Experiments and Spectroscopy for realistic Surface Complexation Modelling of the Sorption of Americium, Curium, and Europium onto Muscovite

Bezzina, J. P.; Neumann, J.; Brendler, V.; Schmidt, M.;

Originally published:

August 2022

Water Research 223(2022), 119032

DOI: https://doi.org/10.1016/j.watres.2022.119032

Combining Batch Experiments and Spectroscopy for realistic Surface Complexation Modelling of the Sorption of Americium, Curium, and Europium onto Muscovite

James P. Bezzina[a], Julia Neumann[a,≠], Vinzenz Brendler[a], and Moritz Schmidt[a*]

[a] *Helmholtz-Zentrum Dresden-Rossendorf (HZDR), Bautzner Landstraße 400, 01328 Dresden, Germany*

[≠] *Current Address: Argonne National Laboratory, 9700 South Cass Ave, Lemont, IL 60439, USA*

* *Corresponding Author, E-Mail address:* moritz.schmidt@hzdr.de

James Paul Bezzina: jamespaulbezzina@gmail.com

Julia Neumann: jneumann@anl.gov (ORCID: 0000-0002-3650-3967)

Vinzenz Brendler: v.brendler@hzdr.de (ORCID: 0000-0001-5570-4177)

Moritz Schmidt: moritz.schmidt@hzdr.de (ORCID: 0000-0002-8419-0811)

Abstract

For a safe enclosure of contaminants, for instance in deep geological repositories of radioactive waste, any processes retarding metal migration are of paramount importance. This study focusses on the sorption of trivalent actinides (Am, Cm) and lanthanides (Eu) to the surface of muscovite, a mica and main component of most crystalline rocks (granites, granodiorites). Batch sorption experiments quantified the retention regarding parameters like pH (varied between 3 and 9), metal concentration (from 0.5 µM Cm to 10 µM Eu), or solid-to-liquid ratio (0.13 and 5.25 $g \cdot L^{-1}$). In addition, time-resolved laser fluorescence spectroscopy (TRLFS) using the actinide Cm(III) identified two distinct inner-sphere surface species. Combining both approaches allowed the development of a robust surface complexation model and the determination of stability constants of the spectroscopically identified species of $(\equiv S\text{-}OH)_2M^{3+}$ ($\log K^e$ −8.89), $(\equiv S\text{-}O)_2M^{+}$ ($\log K^e$ −4.11), and $(\equiv S\text{-}O)_2MOH$ ($\log K^e$ −10.6), with all values extrapolated to infinite dilution. The inclusion of these stability constants into thermodynamic databases will improve the prognostic accuracy of lanthanide and actinide transport through groundwater channels in soils and crystalline rock systems.

Keywords: mica, trivalent actinides, retardation, TRLFS, Diffuse Double Layer Model

Highlights:

- Multi-method approach to study trivalent actinide sorption onto muscovite
- First spectroscopic verification of surface species of trivalent actinides on muscovite
- Reliable surface complexation model based on spectroscopically verified speciation

38 **TOC Graphic:**

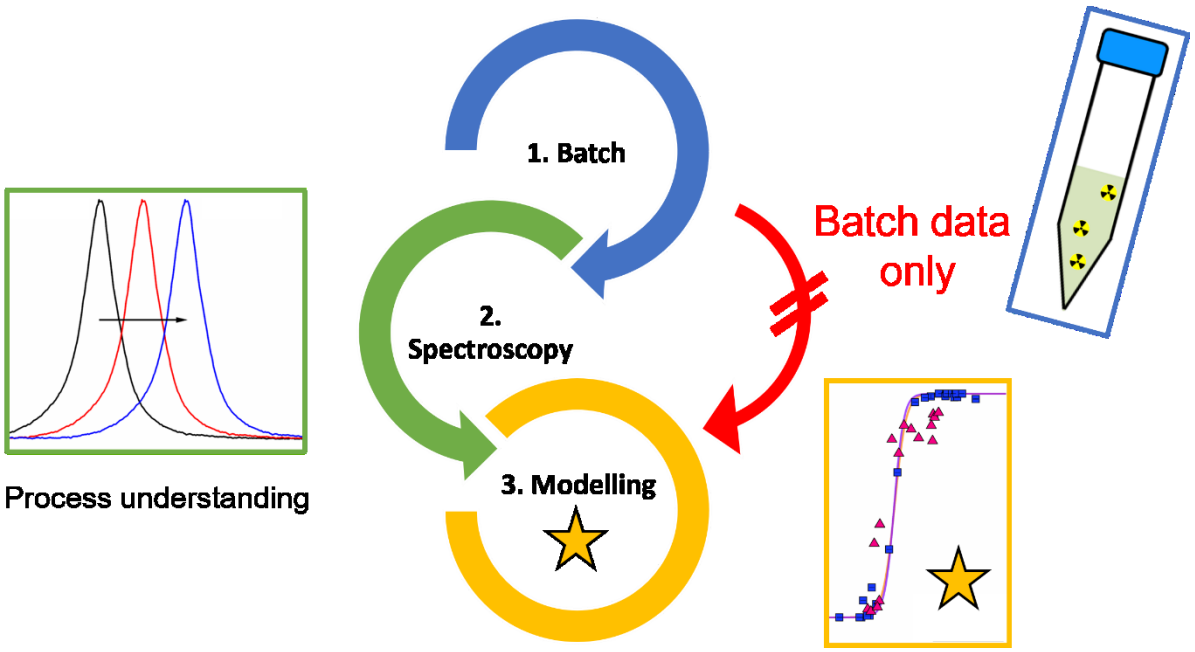

39

40

1. Introduction

Hazardous waste from a manifold of sources must be confined from the ecosphere, and specifically from entering the food chain. Prominent examples are metal ore mining and processing, fertilizer production, nuclear power generation, geothermics, decommissioning of industrial installations, and most branches of consumer good production. To safely dispose of such contaminants for long periods is a huge challenge and of great societal concern. In the case of radioactive waste, safe isolation for 1 million years is demanded by German law to be considered in safety assessments (NEA, 2006). Engineered barriers are usually expected to fail in their protection functions after thousands of years, after which the influx of groundwater will mobilize toxic materials and potentially introduce such species into the water table. In case of radioactive waste, and with the ability for mineralogical formations to retain mobile species, this has led to the consideration of deep geological storage as the most viable option in many countries, such as Russia, Japan, USA, and Germany (Blyth et al., 2009; Ojovan et al., 2019; Vokál et al., 2010). The selection and characterization of a suitable multi-shell encapsulation system (including the host rock) requires serious consideration to prevent transfer of radionuclides into the ecosphere.

Granitic rock is one such formation (BGE, 2020; Laverov et al., 2016; Oy, 2012; Yamamoto et al., 2013) and consists predominantly of quartz, feldspar, and mica in varying ratios. Studies conducted on the immobilization characteristics of complete mineral assemblies will generate information on a specific granite only; alterations in composition may however alter performance between samples. With mechanistic understanding of the sorbing capabilities of individual mineral phases a more universal approach can be generated, further improving predictions for retardation capabilities within complex rock assemblies (Stockmann et al., 2017).

Minor actinides Americium and Curium, but also Plutonium, contribute significantly to the total radiotoxicity of spent nuclear fuel and are expected to occur in their trivalent oxidation state under the strongly reducing conditions developing over time in a deep geological repository. As Pu(III) is a big challenge for experimental designs, many sorption studies have focused on Am(III) and Cm(III), as well as an inactive rare earth analogue Eu(III) – all of them keeping their oxidation state even under oxidizing conditions. Here, interactions with mineral phases such as feldspars (J. Neumann et al., 2021; Stumpf et al., 2006b), clays (Hartmann et al., 2011; Schnurr et al., 2015; Stumpf et al., 2004), and aluminum (Huittinen et al., 2009) and

iron oxides (Stumpf et al., 2006a) as well as quartz (García et al., 2019) are of highest importance. Surface complexation models (SCM) for actinide sorption have also been developed for some of these systems. In a brief overview, quartz was reported to display two distinct adsorbed species ($(\equiv S\text{-}O)_2HEu^+$ between pH ~3.5 and 6 and $(\equiv S\text{-}O)_2EuOH$ as pH increases) that vary in immobilization contribution dependent on ionic strength (García et al., 2019). Feldspar minerals have been reported to display as many as four distinct surface species ($(\equiv S\text{-}OH)_2M^{3+}$, $(\equiv S\text{-}O)_2M^+$, $(\equiv S\text{-}O)_2MOH$ and $(\equiv S\text{-}O)_2M(OH)_2^-$), verified utilizing both SCM and spectroscopy (J. Neumann et al., 2021; Stumpf et al., 2006b).

Mica minerals, such as muscovite, as major components of granitic rock, have been the focus of several studies investigating their retention potential towards radionuclides. Some investigations also covered effects of counter-ions on sorption of trivalent metal ions (Lee et al., 2013; Neumann et al., 2022; Pan et al., 2017; Yan et al., 2013), of co-ions on nano particle formation of tetravalent actinides (J Neumann et al., 2021), or speciation on U(VI) sorption (Arnold et al., 2006; Richter et al., 2016). Most of these studies used large single crystals as substrates, however, and hence there is still a distinct lack of a fundamental understanding of sorption of trivalent actinides (An(III)) and a realistic set of species required to parametrize respective SCMs to close gaps in thermodynamic databases (Richter, 2015). With the utilization of μTRLFS, sorption of trivalent actinides has been discovered to mainly occur along mineral grain boundaries (Blyth et al., 2009; Demnitz et al., 2022; Molodtsov et al., 2021, 2019) in natural granite samples, including those of the mica mineral fractions. Muscovite is a mica mineral that is both abundant and chemically analogous to illite, and weathering processes of this mineral cause the formation of many other clay minerals and colloidal species (Jackson et al., 1948). For example, muscovite is a major component of a variety of soils (Anand and Gilkes, 1987; Wilson, 2004) and also (22 %) of the mineralogical matrix at the Grimsel Test Site (GTS) (Degueldre et al., 1989; Soler and Mäder, 2010), an underground research laboratory facility in a crystalline rock formation in Switzerland, used for research projects related to radioactive waste disposal. *In situ* experiments conducted in a fracture zone at the GTS showed that transport of trivalent actinides (Am, Cm, and Pu) occurred mainly colloid-mediated, in particular through their adsorption to mobile clay colloids (Geckeis et al., 2004; Möri et al., 2003). It, therefore, seems imperative that the behavior of muscovite will be pivotal for an overarching model describing the long-term mobility of disposed (radio-)toxic waste compounds. Hence, this work strives for the formulation of a SCM for the sorption of An(III)/Ln(III) to the surface of muscovite based on a sound molecular-level understanding of

the interfacial speciation. As the data situation with respect to metal cation sorption onto other micas (biotite, chlorite, phlogopite, glauconite) is similarly disappointing, any muscovite sorption model may at least be indicative or serve for scoping calculations also for such systems.

The information derived from such studies will help improve the accuracy of reactive transport models, such as the 'Smart K_d-concept' (Stockmann et al., 2017), which is a modern and robust approach to simulate contaminant transport through complex geochemical systems. The premise behind this concept is the computation of distribution coefficients (K_d values) based on sorption equilibria for each relevant ion-mineral combination in a comprehensive and competitive manner. Such calculations exploit the mechanistic understanding casted into validated surface complexation and ion exchange models. Then, it is easy to perform these computations for a wide range of physicochemical parameters, generating multidimensional matrices. They, in turn, are used in reactive transport codes for a more reliable prediction of contaminant transport through ground water pathways within the host rock, taking into consideration localized geochemical conditions and decreasing the computational costs for each simulation (Stockmann et al., 2017).

This study combines sorption experiments (pH edges and isotherms) with TRLFS investigations in the exploration of trivalent actinide (Am, Cm) and lanthanide (Eu) sorption to the surface of muscovite. In a next step, SCMs are generated with and without the implementation of spectroscopically observed species. The finally selected species set with respective reaction constants are valuable expansions to thermodynamic databases. Namely, they allow for a more realistic description of actinide immobilization by muscovite (e.g. as a major constituent of granitic rock). Thus, our approach provides robust thermodynamic data based on molecular level speciation derived from spectroscopic investigations. Due to the use of multiple trivalent actinides and lanthanides the data are nonetheless generic and can be used to describe the interaction of any trivalent f-elements with muscovite mica. The resulting increased modelling accuracy for long-term safety assessments aids in the selection of sites suitable for deep geological storage of radioactive waste.

2. Materials and Methods

2.1. Materials

For all sorption experiments, NaCl was purchased from Sigma-Aldrich and HCl and NaOH (Sigma-Aldrich) were used for pH adjustments. An ^{243}Am stock solution (in 0.01 M HCl) was diluted for batch contacts, a stock solution of ^{248}Cm in 1 M $HClO_4$ was diluted for TRLFS experiments, and $EuCl_3 \cdot 6H_2O$ (99.9%, abcr Chemie) was used for batch sorption experiments. Milli-Q water was produced via ultrafiltration (membraPure, Astacus^2) and its resistance was measured to be > 18 MΩ.

Synthetic muscovite mica sheets (V1 quality, AFM standard 25×75mm) were supplied by Ted Pella, Inc (Redding, California, USA). The mineral sheets were crushed into platelets by a tungsten carbide ball mill (Fritsch Pulverisette 7 Planetary Micro Mill), then sieved to a size fraction of 20 – 63 µm via dry vibrational sieving (Fritsch Pulverisette 7 sieve). The crystal structure of the mineral was analyzed using Powder X-Ray Diffraction (PXRD, Rigaku MiniFlex600 and the PDXL software suite) and elemental composition was analyzed using X-Ray Fluorescence Analysis (XFA, PANalytical, Axios^{mAX}, Rh X-Ray Source).

Muscovite mica ($KAl_2(AlSi_3O_{10})(OH)_2$) is a phyllosilicate. It displays a TOT layered structure, with an aluminum octahedral layer (O) 'sandwiched' between two silicate tetrahedral layers (T), and a potassium interlayer between sheets. As many common phyllosilicate minerals contain a range of transitional metals, XFA was used for the determination of the mineral's iron concentration (1.9%, Table S1), which is relevant for the interpretation of the TRLFS results (see below).

The specific surface area (SSA, 18.1 $m^2\ g^{-1}$) was measured using N_2-BET analysis (Quantachrome ASiQwin QuadraSorb) and the surface binding site density (SSD, 2.61 sites nm^{-2}) was obtained from literature (Arnold et al., 2001). Zeta potential measurements of the muscovite powder were conducted by first generating a range of 20 samples with a solid:liquid ratio (SLR) of 0.15 g L^{-1} and [NaCl] of 0.1 M, and pH adjustments were conducted by addition of negligible quantities of 1, 0.1, or 0.01 M HCl or NaOH. Suspensions were equilibrated over a 48-h period in an end-over-end agitator, before surface charge measurements were taken by zeta-potential measurements (Malvern Company, Zetasizer Nano ZS). Respective results are reported within the supplemental information (Figure S1).

2.2. Sorption Experiments

2.2.1. Batch sorption experiments - pH edges. Eu(III) batch sorption experiments were conducted by the generation of mineral suspension with an SLR of either 1 or 3 g L^{-1} and metal concentrations of 10 or 0.5 µM Eu(III). All sorption experiments with Eu were performed under atmospheric conditions. The investigated metal concentrations represent typical REE concentrations measured for waste water of REE mining sites (up to 80 µM and lower) (Grawunder et al., 2014; Hao et al., 2016; Merten et al., 2005). Expected concentrations for trivalent actinides in the vicinity of a nuclear waste repository are significantly lower (Keesmann et al., 2005; Zhao et al., 2016). The chosen SLR and metal concentrations correspond to site occupancies of ≤ 18 % (see section 3 in SI for further explanation) assuming a bidentate binding mechanism, at which (surface) precipitation is not expected for pH ≤ 8 (Table S2). The background electrolyte concentration was set to 0.1 M NaCl to maintain constant ionic strength and the pH of each suspension was altered by addition of negligible quantities of 1, 0.1, or 0.01 M NaOH or HCl. Samples were prepared as singlets. After pH adjustment, suspensions were equilibrated for > 48 h by end-over-end agitation in ambient conditions (25 ± 1°C).

Scoping calculations with PhreeqC and the ThermoChimie TDB (version 10a (Blanc et al., 2015; Giffaut et al., 2014; Grivé et al., 2015)) were performed to estimate the amount of Eu potentially transforming into secondary solid phases. The maximum [Eu] considered was 10^{-5} mol/L, in the pH edge experiments at pH 6, beyond which sorption will reduce the Eu content in the aqueous phase significantly. Here, only $Eu(OH)_3$(am) and $Eu(OH)CO_3 \cdot 0.5H_2O$ were assumed relevant as any formation of well-crystalline minerals within only five days and at ambient temperatures is implausible. The saturation indices for the two solids were −5.62 and −5.81, respectively. Therefore no precipitation is expected from a theoretical point of view and indeed no secondary phase formation was observed in any sorption experiment.

^{243}Am experiments were undertaken in a similar manner (SLR of 3 g·L^{-1} and [Am^{3+}] of 10 µM), but in a nitrogen glovebox for radiation protection reasons, and agitation was conducted on an orbital shaker. For all sorption samples, post contact pH of the suspension was measured prior to centrifugation for 20 min (3.46 *g*), and afterwards three aliquots of the supernatant were taken for analysis of remaining metal concentration via ICP-MS

(PerkinElmer LAS; NexION 350X). Displayed error bars represent the standard deviation of the triple ICP-MS measurement. The quantitative information from the Cm(III) TRLFS results was also considered here.

2.2.2. Sorption isotherm experiments. Sorption isotherm experiments were conducted in a similar manner to the batch sorption experiments, however a static pH (pH ~ 7) was decided upon, to minimize mineral dissolution and ensure complete uptake of available Eu^{3+} (> 90 %, see Figure S3 in SI for details). Deviating from the usual isotherm philosophy, [Eu^{3+}] was kept constant at 1.5 µM in order to alleviate concerns of the precipitation of amorphous $Eu(OH)_3$ or $Eu(OH)CO_3 \cdot 0.5H_2O$. The respective saturation indices are −3.55 and 0.26, computed as outlined under section 2.2.1. Assuming no sorption, this would translate into a maximum of about 45% of initial Eu being theoretically precipitated as $Eu(OH)CO_3 \cdot 0.5H_2O$.

Instead of varying [Eu], the SLR was altered between 0.13 and 5.25 $g \cdot L^{-1}$, corresponding to a site occupancy of ~0.75% and ~50%. The minimal SLR investigated (0.13 $g \cdot L^{-1}$) provided a maximum of ~50% theoretical site occupancy (Lützenkirchen and Behra, 1996), also minimizing the risk of surface precipitation.

Mineral suspensions were equilibrated over 48 h in D.I. water before addition of electrolyte solution and pH equilibration (where pH was adjusted as above). After pH remained steady over a 24 h period, suspensions were spiked with a Eu(III) stock solution. If a pH drift was observed during the reaction time, it was adjusted back to the desired pH and contacted until the pH remained stable (±0.05) for a minimum of 48 h. Equilibrated suspensions were centrifuged and analyzed in the same manner as those within the batch sorption experiments.

Sorption isotherm data were fit to three common two-parameter models. In brief, the Freundlich model is described by the following equation (Dada et al., 2012; Ho et al., 2002):

$$q_e = a_F C_e^{bF} \qquad \text{(Eq. 1)}$$

It contains two constants, the relative adsorption capacity, a_F and the heterogeneity factor or intensity of binding, b_F (both unitless) (Dada et al., 2012); where a value of ≥ 1 alludes to multi-layer sorption, ≤ 0 alludes to irreversible binding, and $1 > b_F > 0$ describes the homogeneity (the higher the value the more heterogeneous, potentially displaying multiple bound species).

With respect to the Langmuir isotherm:

$$q_e = \frac{q_m a_L C_e}{1+a_L C_e} \quad \text{(Eq. 2)}$$

the monolayer sorption equilibrium constant is given by a_L ($L \cdot m^2 \cdot mol^{-1}$), and the value of q_m ($mol \cdot m^{-2}$) relates to the equilibrium sorption capacity (Ho et al., 2002).

Lastly, we applied the Dubinin–Radushkevich (D-R) model (Ho et al., 2002):

$$q_e = q_D exp\left(-B_D\left(RT \cdot ln\left(1+\frac{1}{C_e}\right)\right)^2\right) \quad \text{(Eq. 3)}$$

, which describes both, the homogeneous binding capacity (q_D, $mol \cdot m^{-2}$) and the energies of binding E ($kJ \cdot mol^{-1}$), and therefore further mechanistic information (B_D):

$$E = \frac{1}{\sqrt{2B_D}} \quad \text{(Eq. 4)}$$

, where sorbent-sorbate interactions can be elucidated ($E < 8$ $kJ \cdot mol^{-1}$ equates to physisorption/ outer-sphere sorption (Van der Waals interactions), 8 $kJ \cdot mol^{-1} < E < 16$ $kJ \cdot mol^{-1}$ equates to intermediate cases and $E > 16$ $kJ \cdot mol^{-1}$ equates to chemisorption/ inner-sphere sorption (Bulai et al., 2009).

2.3. Time-Resolved Laser-Induced Fluorescence Spectroscopy (TRLFS)

For structural investigations, the actinide Cm(III) was used as a luminescent probe at a concentration of 0.5 µM at an SLR of 3 g L^{-1} in the pH range 4.5 – 7.5. The sample preparation was performed within a glove box under nitrogen atmosphere for radiation safety reasons. A pulsed (5 – 8 ns) Nd:YAG OPO laser system (Powerlite Precision II 9020) coupled with an OPO (PANTHER EX OPO, Continuum, USA) was used for excitation of the sample, at the most intense adsorption line ($^8S_{7/2} \rightarrow {}^6I_{11/2}$) of Cm(III) at 396.6 nm, within a quartz cuvette. The luminescence was collected using an optical fiber and transferred to a 300 lines/mm grating polychromator (Andor Kymera-328I-C) and CCD Camera (iStar DH320T-18U-63). A delay between the laser pulse and luminescence measurement of 1 µs was generated (DG535 Digital Delay Generator, Stanford Research Systems, Inc.) for protection of the detector from intense pulses.

With increasing complexation of Cm(III), a red-shift of the emission band with respect to the Cm(III)-aquo ion (593.8 nm) is observed. Therefore, from the spectral deconvolution of emission spectra the Cm(III) speciation can be obtained, with the band positions of single

component spectra giving information about their chemical environment. With the change in the emission band, also a shift of the absorption maximum of each species is observed. Therefore, the efficiency of the luminescence excitation is reduced. To deduce the relative abundances of the distinct chemical species, their contribution to the overall speciation needs correction by relative fluorescence intensity (FI) factors (Edelstein et al., 2006). Furthermore, the lifetime of this luminescence is also highly dependent on the hydration shell of Cm(III), and with analysis of this lifetime the number of waters within the hydration shell can be determined (Kimura et al., 1996).

There are, however, limitations of this approach to speciation determination. The first of which is that both the Cm aquo ion and its outer-sphere sorption complex will return the same emission spectra, as neither species display alteration of the inner hydration sphere; the second is that with the presence of transition metals (specifically iron) in the mineral sample, relaxation processes will quench the luminescence by non-radiative energy transfer (Hartmann et al., 2008). This quenching process will decrease the reliability of both lifetime analysis and FI calculation. FI factors for mineral sorption species can, however, be calculated from the species' band position using the relationship described in Eibl *et al.* (Eibl et al., 2019).

2.4. Surface Complexation Modelling (SCM)

The determination of the surface complexation parameters was conducted through coupling the geochemical speciation software PhreeqC (version 3.6.2.15100, (Charlton and Parkhurst, 2011; Parkhurst and Appelo, 2013) and the parameter estimation code UCODE 2014 (version 1.004 (Poeter et al., 2014)). A diffuse double layer model was applied (Dzombak and Morel, 1990). For aqueous speciation of Eu(III), Cm(III), and Am(III) as well as mineral dissolution thermodynamic data, the ThermoChimie PhreeqC TDB (version 10a (Blanc et al., 2015; Giffaut et al., 2014; Grivé et al., 2015)) was used. The surface of muscovite was considered to contain one generic functional group (surface site ≡S-OH) with protolysis values pK_a taken from literature (Arnold et al., 2001), i.e. valid at their experimental ionic strength of 0.1 M, being identical to the one in this work:

$$\equiv S\text{-}OH + H^+ \rightleftharpoons \equiv S\text{-}OH^+_2 \qquad pK_1 = 6.06 \qquad \text{(Eq. 5)}$$

$$\equiv S\text{-}OH \rightleftharpoons \equiv S\text{-}O^- + H^+ \qquad pK_2 = -7.81 \qquad \text{(Eq. 6)}$$

An overview of the thermodynamic parameters used in the SCM is given in **Table 2**.

3. Results

3.1. Batch Sorption Experiments

3.1.1. Aqueous speciation. The aqueous speciation of each system (Am(III), Cm(III) and Eu(III)) were calculated at experimentally relevant conditions using PhreeqC (see section 5 in SI). M^{3+} is the predominant species in all data series up to a pH of ~7.5, where it is overtaken by hydrolysis products ($M(OH)^{2+}$ or $M(OH)^{+}_2$). Between pH ~8.5 – 10, $M(OH)_2^{+}$ is the most dominant species in each case before being overtaken by $M(OH)_3$ at pH 10.5 for Eu(III). As we have limited the pH range to pH < 9, the neutral species can thus be neglected. The introduction of carbonate changes the speciation slightly, especially under alkaline pH conditions, with the MCO_3^{+} complex being dominant for pH 8 – 8.5. As experiments with Am(III) were conducted under exclusion of atmospheric CO_2, any influence of carbonate complexation should be visible as differences between the Eu(III) and Am(III) data in this pH range. Moreover, carbonate complexation – in solution or as a ternary complex on the muscovite surface – should be easily identifiable by Cm(III) TRLFS (Kim et al., 1994; Marques Fernandes et al., 2010).

3.1.2. pH edges. The sorption data of Eu(III) and Am(III) (spectroscopically observed Cm(III) sorption data has been also included) are reported on the surface of muscovite flakes (< 63 μm). In order to gain insight into site occupancy effects on the sorption edge, two SLR (1 and 3 $g \cdot L^{-1}$) and two concentrations ($[Eu^{3+}]$ = 0.5 and 10 μM) were investigated, with an extension to Am(III) (10 μM $[M^{3+}]$, SLR of 3 $g \cdot L^{-1}$) and Cm(III) (0.5 μM $[M^{3+}]$, SLR of 3 $g \cdot L^{-1}$). The percentage immobilization as a function of pH is given in **Figure 1**.

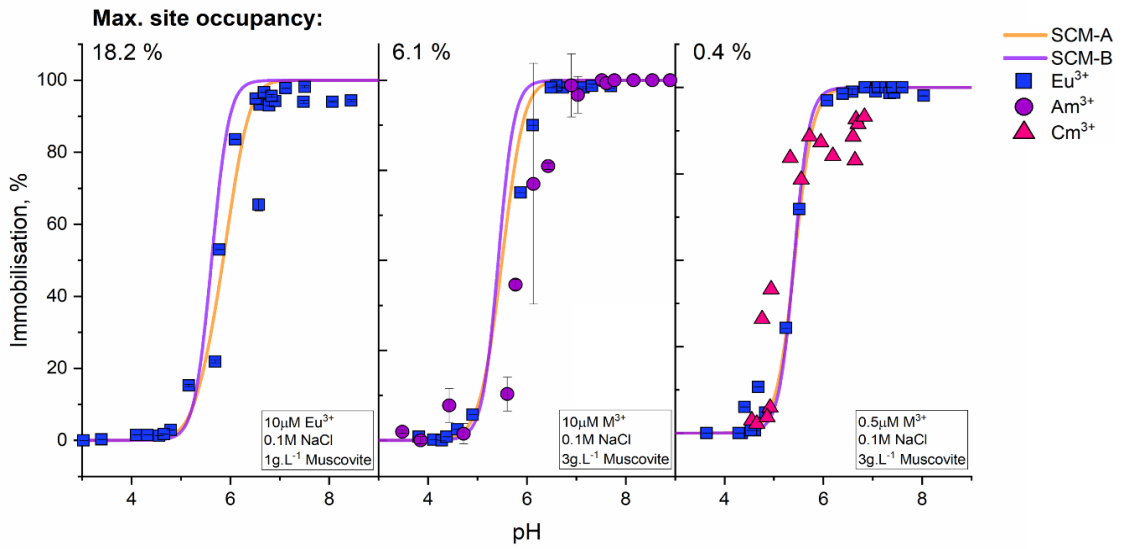

297

298 **Figure 1:** Batch sorption data (symbols), underlaid by the calculated speciation by the
299 developed SCMs (cf. section 3.3, solid lines), for the sorption of Am(III) and Eu(III) to the
300 surface of muscovite flakes (< 63 µm) in the given experimental conditions. Additionally,
301 retention of Cm(III) based on spectroscopic investigations is plotted for comparison (cf. section
302 3.2). Reported error bars represent the uncertainty of triplet ICP-MS measurements and are
303 smaller than the plotted symbols.

304 Eu(III) immobilization on muscovite begins at pH ~5 and reaches 100 % by a pH of ~6.5
305 (**Figure 1**). The obtained sorption edges show a small shift towards lower pH with decreasing
306 maximum site occupancy (**Figure 1**, left to right). One noticeable deviation is observed for the
307 spectroscopically derived Cm(III) data (see below) at highest pH values (pink symbols in
308 **Figure 1**, right). While both Am(III) and Eu(III) reach a plateau at 100% immobilization at pH
309 ~6.5, the plateau for Cm(III) begins at the same pH but only reaches ~90% immobilization,
310 which is likely caused by the presence of ~10 % outer-spherical bound Cm. This is because it
311 is impossible to distinguish outer-sphere complexes from the aquo ion by TRLFS due to the
312 lack of changes in the first hydration shell of Cm. The data for Eu(III) measured in normal
313 atmosphere and the Am(III) data measured under N_2 atmosphere are identical within the
314 precision of the measurement, suggesting no influence of carbonate on the sorption process. A
315 confirmation of this assumption on the molecular level will, however, have to rely on
316 spectroscopic data.

317 *3.1.3. Sorption isotherms*. The isotherm data is plotted in **Figure 2** with q_e (equilibrium
318 concentration of Eu(III) adsorbed on the mineral surface, $mol \cdot m^{-2}$) as a function of C_e

(equilibrium solution phase concentration of Eu(III), adjusted for available mineral surface area, mol·L^{-1}·m^2). This data plot is combined with fitted Langmuir, Freundlich, and D-R isotherms.

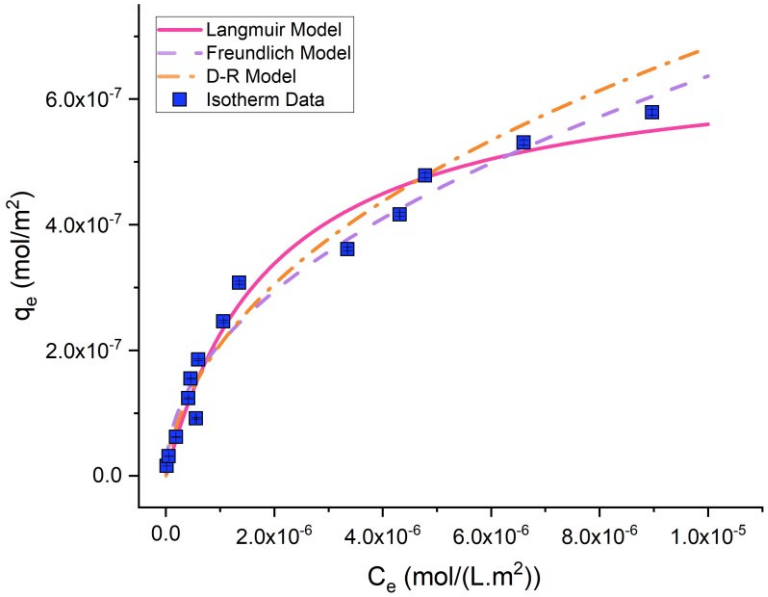

Figure 2: Equilibrium isotherm of Eu(III) sorption to the surface of muscovite (pH 7 ± 0.05, 1.5 µM Eu(III)), with respective fits to Langmuir, Freundlich, and D-R isotherm models. Reported error bars represent the uncertainty of triplet ICP-MS measurements and are smaller than the plotted symbols.

Sorption of Eu(III) to muscovite displays an initially steep isotherm profile, indicative of strong sorption. Beyond a C_e of $2.0 \cdot 10^{-6}$ mol m^{-2} this profile begins to display a gentler slope, while not levelling out completely. This alteration in isotherm profile is coupled with a slow approach to adsorption saturation of the surface, as extraction efficiency decreases from 100% to ~90% (Figure S3). The values generated by fitting the isotherm data to the models (cf. section 2.2.2.) are reported within **Table 1**.

Table 1: The three common two-parameter models for the description of the isotherm data obtained within this study. Errors given are calculated from the square root of the diagonals of the covariance matrix and correspond to two standard deviations.

Model	Parameter	Value
Freundlich	a_F	$2 \pm 1 \cdot 10^{-4}$
	b_F	0.48 ± 0.06
	R^2	0.970
Langmuir	a_L / (L.m^2)·mol^{-1}	$5 \pm 1 \cdot 10^5$

	q_m / mol·m^{-2}	$6.7 \pm 0.8 \cdot 10^{-7}$
	R^2	0.972
D-R	q_D / mol·m^{-2}	$1.0 \pm 0.4 \cdot 10^{-5}$
	B_D	$3.3 \pm 0.4 \cdot 10^{-9}$
	E / kJ·mol^{-1}	12.3 ± 0.6
	R^2	0.972

329

330 The sorption data were reasonably well-fit to all three models ($R^2 \geq 0.97$). The fits to the
331 Freundlich isotherm relate to a strong binding mechanism (b_F of 0.48), leading to the
332 determination that within the site occupancy range studied, no surface precipitation or
333 cooperative binding (multi-layer) mechanism was apparent.

334 The Langmuir model returns an equilibrium sorption capacity q_m of $6.7 \pm 0.8 \cdot 10^{-7}$ mol·m^{-2},
335 which slightly exceeds the maximum equilibrium concentration of adsorbed Eu(III) (q_e) on the
336 mineral surface covered by our measurements (~$6.0 \cdot 10^{-7}$ mol·m^{-2}). Despite this extrapolation
337 of the experimental data the Langmuir model is still a reasonable descriptor of the data at hand.

338 In stark contrast, the homogeneous binding capacity q_D for the D-R isotherm is
339 $1.0 \pm 0.4 \cdot 10^{-5}$ mol·m^{-2} and is based on a much larger extrapolation of this data (see orange
340 curve in Figure 2), leading to very tentative reliance on this model. In other words, the result
341 of our isotherm analysis overestimates the amount of sorption, since the homogeneous binding
342 capacity is 2-3 times larger than the total number of available sorption sites according to the
343 SSD used in our SCM (2.61 sites·nm^{-2} corresponding to $4.33 \cdot 10^{-6}$ mol·m^{-2} (Arnold et al.,
344 2001)). It is possible that a contribution of outer-sphere species leads to the high value of q_D as
345 outer-spherically bound species do not occupy specific sorption sites. The E value determined
346 from the D-R isotherm model of 12.3 kJ·mol^{-1} is in between the typical energies of
347 physisorption and chemisorption, which can be interpreted as a combination of both processes,
348 consistent with the interpretation of the value for the homogeneous binding capacity.

349 In short, while details vary between different isotherms, all models describe a strong,
350 heterogeneous binding mechanism. Both the Freundlich and Langmuir isotherms describe a
351 process that occurs in the absence of any precipitation. This, in conjunction to a high
352 heterogeneity factor and a D-R binding energy between physisorption and chemisorption, leads
353 to the allusion of multiple reactions causing sorption of Eu(III) onto the surface of muscovite.
354 With these assumptions in mind, it can be assumed that there is a combination of both outer-

sphere (physisorption) and inner-sphere sorption (chemisorption) mechanisms creating the measured sorption profiles.

3.2. Time-resolved laser-induced fluorescence spectroscopy (TRLFS)

By TRLFS measurement using the luminophore Cm(III), we are able to gain insight into the speciation and potentially the sorption mechanism of An(III)/Ln(III) on muscovite. As the position of the $^{6}D_{7/2} \rightarrow {}^{8}S_{7/2}$ luminescence band shifts depending on the chemical environment of Cm(III), the peak deconvolution of the measured Cm emission spectra enables the identification of the present species and their quantitative contributions to the overall speciation (Eibl et al., 2019; Huittinen et al., 2012; Stumpf et al., 2001). With this information, further deductions can be made upon the mechanisms of sorption of An(III)/Ln(III). The spectra utilized in deconvolution, residual spectra after deconvolution, and deconvoluted single component spectra are plotted in **Figure 3**. Due to the iron content of the muscovite samples (Table S1), the signal-to-noise ratio of the emission spectra was relatively low. And, while lifetimes can be derived from our data, they do not contain the structural information with respect to the number of water molecules in the Cm's first coordination sphere, due to the excess quenching effect of structural Fe.

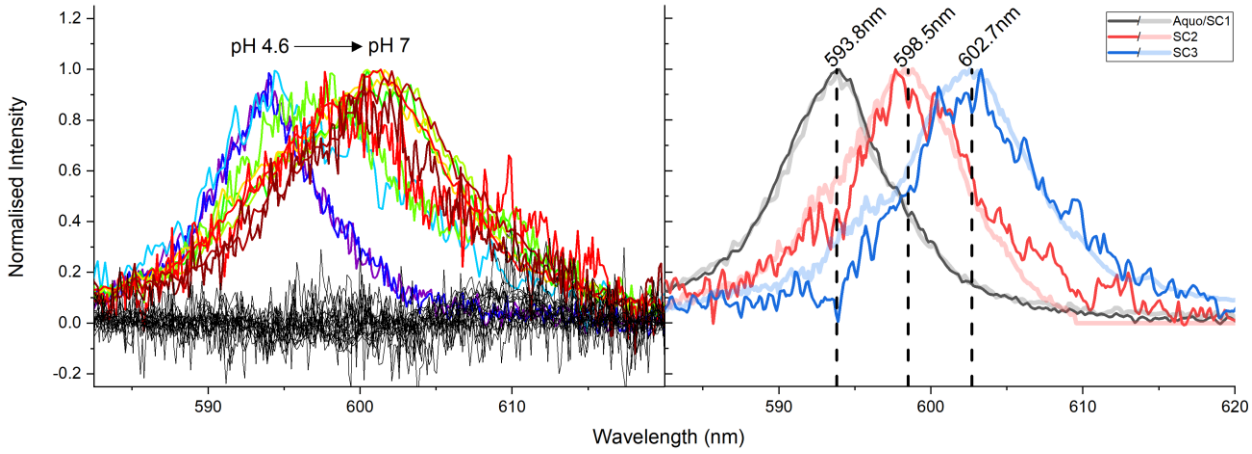

Figure 3: Emission spectra of Cm sorbed to the surface of muscovite between pH 4.6 and 7 (left) and the single component spectra (right) deconvoluted for each species within this study (solid, lines) underlaid by the respective single component spectra for Cm(III) adsorbed on K-feldspar deconvoluted within Neumann et al. (J. Neumann et al., 2021) (translucent lines).

In addition to the Cm(III) aquo ion, a minimum of two distinct species were required in order to minimize the residual spectra (**Figure 3** left, black) after deconvolution. These species have been assigned as an inner-sphere surface complex (SC) of Cm(III) (SC2, $(\equiv S\text{-}O)_2M^+$, peak at ~598 nm) and its hydrolysis species (SC3, $(\equiv S\text{-}O)_2MOH$, peak at ~603 nm), by referencing similar studies on K-feldspar (J. Neumann et al., 2021), illite/montmorillonite (Schnurr et al., 2015), and kaolinite (Huittinen et al., 2012, 2010). Deconvolution of individual species' spectra became difficult, due to the simultaneous occurrence of multiple species, overall low signal quality, as well as a potential small contribution (< 5%) of a fourth species. Therefore, deconvolution was conducted based on single component spectra available in the literature for the sorption of Cm(III) on another alumina-silicate mineral, K-feldspar (J. Neumann et al., 2021). These spectra are shown as translucent lines in **Figure 3** *(*right).

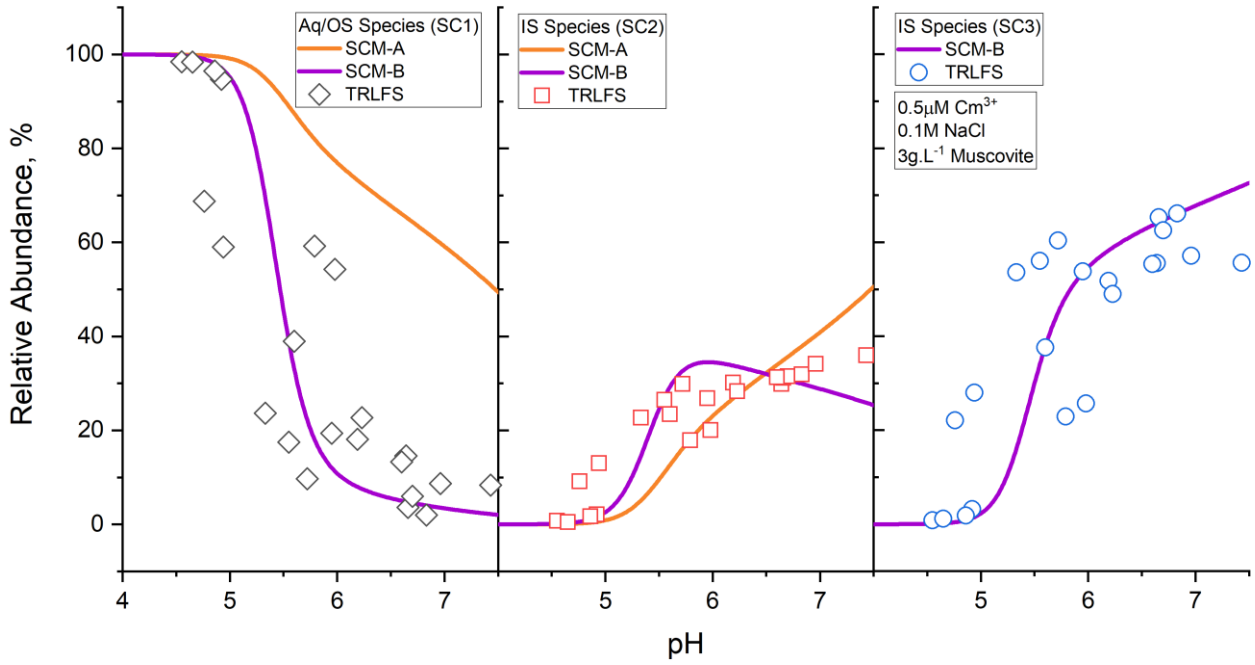

Figure 4. Comparison of the Cm(III) speciation determined through spectroscopic measures (symbols) and the speciation calculated from the surface complexation models of this study (SCM-A and SCM-B, lines). OS: outer-sphere species.

The peak deconvolution resulted in a quantitative species distribution (**Figure 4**), which was corrected by FI values (aquo ion: 1.0, SC2: 0.54, SC3: 0.29, (J. Neumann et al., 2021)). The contribution of spectroscopically indistinguishable Cm aquo ion/outer-sphere species (SC1, **Figure 4**, left) decreases steeply from 100 % at pH ~5 to 10% at pH ~6, from here there is a

steady decrease to > 5% beyond pH 7. As discussed above, complete uptake is observed in batch sorption experiments under identical experimental conditions. Therefore, the observation of a small amount of fully hydrated Cm can be interpreted as a constant contribution of outer-spherically bound Cm to the speciation.

The species designated SC2 (**Figure 4**, middle), present from pH ~5 and higher, is assumed to be analogous to the bidentate inner-sphere sorption species reported for the K-feldspar, $(\equiv S\text{-}O)_2M^+$, displaying a gentle onset, reaching a relative abundance of ~40 % at pH ~6. Parallel to the formation of SC2 its first hydrolysis product, $(\equiv S\text{-}O)_2MOH$ (SC3, **Figure 3**, right), is formed and reaches a maximum relative abundance of ~70 % by pH 7, being the most abundant of the spectrally observable species. There is no evidence of carbonate complex species in solution or on the mineral surface. At those pH values where relevant carbonate concentrations would be expected most Cm(III) has already been adsorbed to the surface. Consequently dissolved carbonate complexes can only play a minor role and are not observed spectroscopically. Ternary surface complexes involving carbonate should exhibit larger red shifts (> 606 nm) (Marques Fernandes et al., 2010), than were found in our experiments. Due to the low signal-to-noise ratio we cannot unambiguously conclude that such species do not form, but it appears evident that they are at most minor species under these conditions.

3.3. Surface Complexation Modelling (SCM)

The surface complexation model was developed utilizing two distinct methods, building on each other. Both models have in common that they postulate bidentate species, because the entropic effect should favor the formation of bidentate complexes (Wang and Giammar, 2013). The first modelling approach (SCM-A) is stepwise, increasing the number of surface species, in order to both describe the batch sorption data and minimize the total number of surface species. It is empirical as it does not take into account specific spectroscopic information. Consequently, SCM-A was initially attempted with a single surface species, increasing the complexity of the system as additional species were included. Stoichiometry of each species was based upon the aqueous speciation within the pH region of the conducted batch sorption experiments (Figure S2).

The second modelling approach (SCM-B) further expands the SCM-A basis. It incorporates spectroscopically observed species in combination with the batch sorption data for the formation of the initial species estimation within the model. The comparison of both models to experimental data is shown in **Figure 1**. Modelled species and their corresponding log K values

are reported in **Table 2**. The nomenclature denotes the level of hydrolysis of sorbed Eu(III), with SC1 being the potential outer-sphere complex not releasing any protons upon formation.

SCM-A, i.e. the model without consideration of the spectroscopic data, showed that two distinct species were sufficient to describe the experimental batch sorption edges of Eu(III) and Am(III), (**Figure 1**). These two major species were assigned as a) an outer-sphere species (SC1), dominating the surface speciation until pH ~6 (Figure S6). However, when comparing the experimentally observed and simulated contributions of these two species (**Figure 4**), it becomes obvious that there are major deviations, in particular SCM-A overestimates dramatically the amount of outer-sphere sorption, which can be easily seen by the orange line in **Figure 4** left, which displays the sum of Cm aquo ion and outer-sphere sorption. Including additional surface complexes within the model led to either the repression of these species to an abundance of zero throughout the fitting, or failure of the modelling process to determine a suitable fit at all. This behavior illustrates the necessity to provide speciation data derived independent from the modelling process, which is why we include the spectroscopically obtained speciation in the next step.

Table 2: Surface complex formation constants of M(III) adsorbed on muscovite, determined via SCM within this study (upper/lower 95% confidence level). The last column gives the values extrapolated to infinite dilution based on Davies, 1962:

Species	Complex formation	logK (SCM-A)	logK (SCM-B)	$logK^{e}$ (SCM-B)*
SC1	$2 \equiv S\text{-}OH + M^{3+} \rightleftharpoons (\equiv S\text{-}OH)_2M^{3+}$	8.57 (8.72/8.42)	7.93 (8.28/7.57)	8.89 (9.24/8.53)
SC2	$2 \equiv S\text{-}OH + M^{3+} \rightleftharpoons (\equiv S\text{-}O)_2M^{+} + 2\ H^{+}$	-5.32 (-5.06/-5.58)	-4.86 (-4.81/-4.92)	-4.11 (-4.06/-4.17)
SC3	$2 \equiv S\text{-}OH + M^{3+} + H_2O \rightleftharpoons (\equiv S\text{-}O)_2MOH + 3\ H^{+}$	-	-11.3 (-11.2/-11.5)	-10.6 (-10.5/-10.8)

* For calculations only model SCM-B should be used!

With the incorporation of the spectroscopically determined speciation, i.e. SCM-B, the upper region of the modelled sorption edge is shifted to slightly lower pH. Both models were capable of describing both inner- and outer-sphere surface complexes. However, considering spectroscopic data, SCM-B also incorporated SC3, see **Figure 4** (purple lines). Consequently, the abundance of SC2 was greatly reduced in place of SC3.

4. Discussion

The sorption edges recorded for Am(III), Cm(III), and Eu(III) overlap with regards to similar suspension conditions, reaffirming the assumptions of analogous behavior of An(III)/Ln(III) (Lee et al., 2006). While the directly comparable analysis of Am(III) and Eu(III) reproduced identical sorption edges, there is a slight discrepancy between those of Am(III)/Eu(III) and Cm(III). This is caused by the two different experimental approaches and the fact that differentiation between Cm aquo ion and outer-sphere complexes within the TRLFS data is impossible. With an inclusion of the spectroscopic data, all three site occupancies are well described by the SCM.

The aqueous speciation of each An(III)/Ln(III) (e.g. hydrolysis or carbonate complexation, Figure S2) appears to have little effect on the sorption behavior, although spectroscopic data shows that hydrolysis does occur at the interface. The transition from M^{3+} to MOH^{2+} or MCO_3^{+} in solution occurs between pH 7 and 8, while sorption in each case begins already at or below pH 5, reaching near completion by pH 6. Previous studies have noted sorption occurring earlier and reported contributions by outer-sphere sorption at the lower pH values (Pan et al., 2017; Yan et al., 2013). This feature is less apparent within this study (~ 10% based on the difference between TRLFS and batch experiments), as Cm-TRLFS returned spectrally observable sorption (inner-sphere) within all pH regions that had also displayed sorption within the batch experiments (**Figure 4** and S4). The spectroscopically derived speciation of Cm(III), however, suggests that outer-sphere complexes do contribute to Cm's speciation albeit in limited quantities.

The fit of the sorption raw data to a variety of isotherm models provided a rather consistent picture. With reference to the Freundlich isotherm results, the heterogeneity factor obtained ($b_F = 0.48 \pm 0.06$) is indicative of a monolayer system, which is in agreement with the reasonable fit towards the Langmuir isotherm model. This value for b_F is, however, skewed closer towards a heterogeneous binding mechanism. Coupled with the variation from the previously determined Langmuir sorption constant (at a higher pH (Yan et al., 2013)) and a high D-R free energy of binding (12.3 ± 0.6 $kJ \cdot mol^{-1}$), a strong indication for multiple mechanisms is provided. This coincides nicely with the independent spectral indication of both inner- and outer-sphere complexes contributing to this sorption process. Thus, these three isotherm models have all acted in support of assumptions corresponding directly to previous understanding of the muscovite system, where multiple species are bound to the surface (Pan et al., 2017; Yan et al., 2013).

Although the batch sorption data is generally well reproduced by SCM-A, a comparison to the spectroscopically derived speciation clearly shows that the abundance of the outer-sphere sorption complex is greatly overestimated by this model (**Figure 4**). Consequently, an inclusion of spectroscopic information (SCM-B approach) led to the identification of one more surface species than dictated within SCM-A. Observation of single component Cm(III) TRLFS spectra displayed a discrepancy between inner-sphere sorption species and batch sorption edge, which was used for the determination of an outer-sphere species. The deconvoluted, single component spectra align well with the spectra previously determined for K-feldspar (J. Neumann et al., 2021), emphasized as they are underlaid within **Figure 3**; alluding to close parallels to the surface speciation between the two alumino-silicate mineral phases.

The formation of a similar surface bound Cm(III) species (∼597 – 599 nm) has been noted between pH 4 and 7 for many alumino-silicate minerals (Huittinen et al., 2012; J. Neumann et al., 2021; Schnurr et al., 2015), with this species appearing at a higher wavelength (∼601 nm) and at pH ∼5 for quartz and for alumina minerals (Kupcik et al., 2016; Rabung et al., 2006). Other studies have postulated secondary hydrolysis species (∼605 – 607 nm) at pH > 8 (Huittinen et al., 2012; Kupcik et al., 2016; J. Neumann et al., 2021; Rabung et al., 2006) and ternary surface complexes (~610 nm) at pH values of 10 and higher (Huittinen et al., 2012). While neither were observed in appreciable amounts within this study, there is the potential for a low abundance (5 %) of a secondary hydrolysis species SC4 (Figure S4), also in our system, however outside of the experimentally investigated range.

From spectroscopic data it is observed that inner-sphere sorption of Cm(III) to the surface and the formation of surface-bound $Cm(OH)^{2+}$ coincide. This species, SC3, swiftly becomes the dominant surface species, and remains so throughout the pH region studied; this occurs despite the low concentration of aqueous $Cm(OH)^{2+}$.

As would be expected with the inclusion of this data, and as has been previously observed (J. Neumann et al., 2021), the approach taken in SCM-B results in a model that displays a better agreement with the spectroscopically observed speciation of Cm(III), while still reproducing the sorption edges with similar accuracy. Thus it is clear that SCM-B is significantly closer to reality than SCM-A. Although the level of description of total sorption is comparable, the extrapolative capability of SCM-B should be much more dependable. To verify that statement, independent sets of sorption data have been tested with experimental parameter ranges differing from those in this study.

Model Validation

For the validation of the models, two previously reported datasets for sorption of lanthanides Nd(III) and Eu(III) to the surface of muscovite flakes were compared with prognostic PhreeqC calculations of the currently developed SCM, utilizing the experimental conditions outlined with each dataset. The first of the two datasets is from a doctoral thesis of C. Richter (Richter, 2015). From this thesis, the immobilization of Nd(III) by a muscovite powder (particle size 30 – 400 µm, 10 % montmorillonite, SSA = 0.66 m^2/g (Britz, 2018; Richter, 2015)) is plotted as a function of pH and has been directly compared to SCM-A and SCM-B from this study in **Figure 5**.

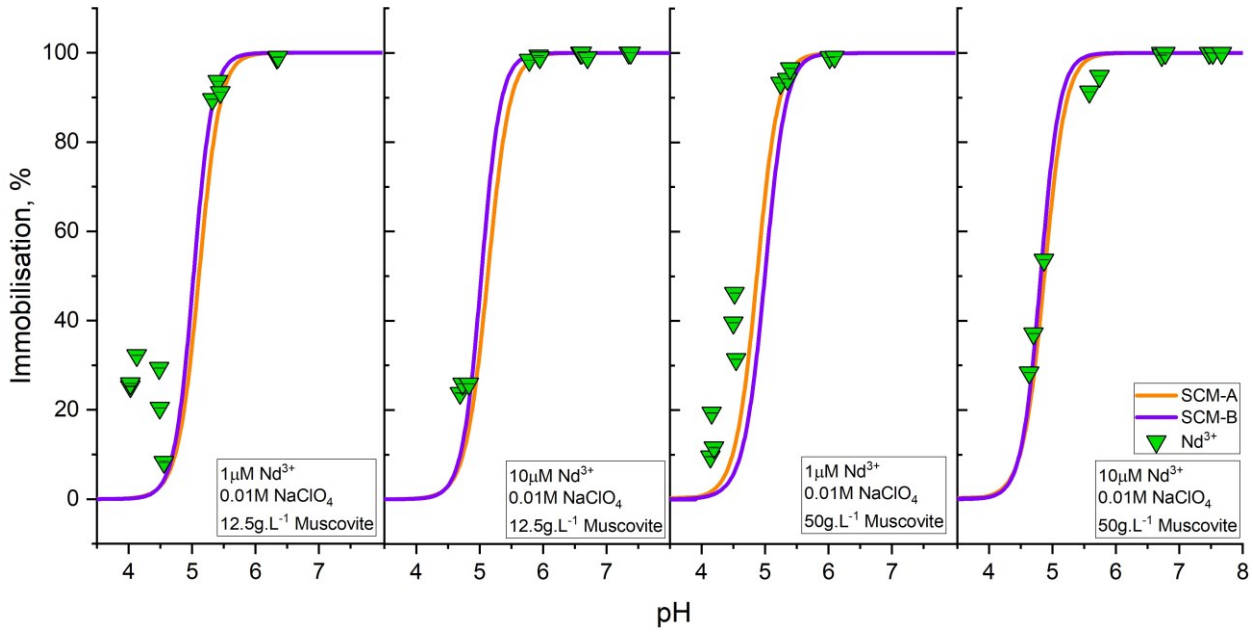

Figure 5: Sorption data of Nd(III) to the surface of muscovite in suspension reproduced from (Richter, 2015) (experimental conditions given in each figure) combined with blind prediction sorption curves utilizing the SCM-A and B approaches from this work.

SCMs developed in this work excellently reproduce the data obtained from this thesis, in particular for points along the top and middle of the sorption edge above pH ~4.5. Both models in each case created a reasonable approximation of the edge, independent of An(III)/Ln(III), ionic strength, or SLR. However, it is difficult to make assumptions about the description of the low pH region of each sorption edge. This agreement of the model derived from Am(III)/Cm(III)/Eu(III) data with Nd(III) sorption data thus not only validates the SCM derived here, but again reaffirms the robust nature of the analogy between Ln(III) and An(III) exploited here and in many other investigations.

529

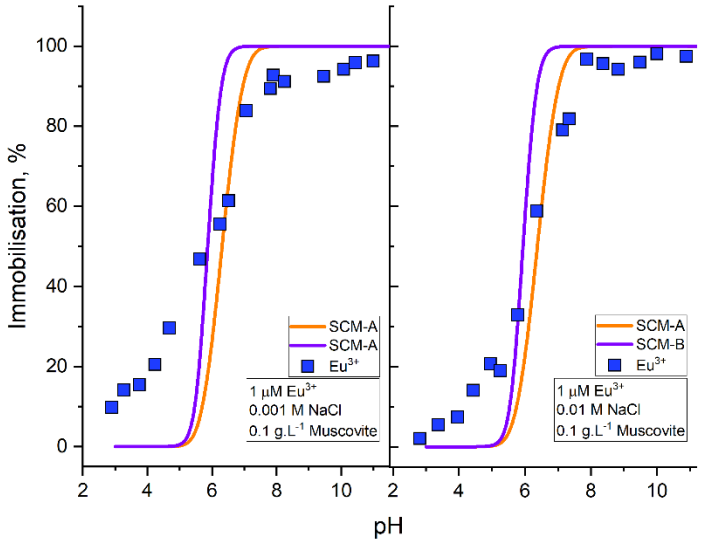

530

Figure 6: Sorption data of Eu(III) to the surface of muscovite in suspension reproduced from Pan *et al.*, 2017 (experimental conditions given in each figure, muscovite flake size: 45 µm, SSA: ~8.9 $m^2 \cdot g^{-1}$) underlaid by the sorption determined by the developed SCM-A and B.

531 The Eu(III) sorption edge of an analogous study, comparing the effects of counter ions on the
532 sorption of Eu(III) to the surface of muscovite by Pan *et al.* (2017), has been digitized and is
533 displayed in **Figure 6**, again underlain with the respective PhreeqC simulations (SCM-A and
534 SCM-B). In this case, however, neither SCM was capable of describing the data satisfactorily.
535 It can be seen that the sorption edge is less steep than predicted by the model. This could
536 potentially be caused by the larger site occupancy in the study of Pan *et al.*, 52 % (as opposed
537 to the maximum of max. ~30 % studied here), which may lead to a higher contribution of outer-
538 sphere sorption, especially at low pH, where the least number of deprotonated sites are
539 available. Another factor relates to a potential inability for our models to describe a relationship
540 between sorption and ionic strength, as the batch sorption experiments only covered one
541 specific ionic strength of 0.1 M. This ionic strength was sufficient for the anticipated
542 application cases for crystalline rocks and soils, where higher ionic strengths are unlikely to
543 occur. However, additional experiments would be necessary when dealing with various clay
544 rocks where higher salinity can be expected, as well as for crystalline rock layers in immediate
545 contact with salt rocks. In such cases, a switch from the Diffuse Double Layer SCM to a
546 Constant Capacitance SCM may be necessary as the latter one is more suitable for higher
547 salinities (Hayes et al., 1991).

5. Conclusions

Here we report the sorption of trivalent europium, americium, and curium by muscovite mica using a multi-method approach, consisting of batch sorption experiments, TRLFS, and SCM. Sorption is low (< 5 %) up to pH 5 but shows a strong increase up to completion around pH 6. All sorption pH edges can be reproduced adequately with only two surface complexes (SCM-A), one outer- and one inner-sphere species.

However, Cm(III) TRLFS revealed the sorption structure on the molecular level and three sorption species were identified: an outer-sphere complex (~10%) at low pH (pH < 6), an inner-sphere complex ($(\equiv S\text{-}O)_2M^+$), and its subsequent hydrolysis species ($(\equiv S\text{-}O)_2MOH$), which form at the same pH. The improved thermodynamic model SCM-B is more realistic and thus more robust with respect to extrapolation beyond the boundary conditions of these experiments, as was proven by modelling independent literature data. SCM-B, therefore, delivers surface complexation parameters (cf. **Table 2***)* that are added to the sorption database of the Smart K_d-concept (Stockmann et al., 2017).

Sorption isotherms delivered thermodynamic parameters of the sorption reaction and support the modelled binding mechanisms. All findings imply great similarities to sorption on K-feldspar regarding sorption quantity and structure.

Overall, the SCM developed within this study will aid in developing transport models for rare earth elements and trivalent actinides in the environment, whenever aqueous media play an essential role. This is relevant for a broad variety of applications, such as safety assessments for nuclear waste repositories, where adsorption of trivalent actinides to mobile clay colloids may increase radionuclide transport. Beyond that the results of this study are also relevant for NORM problems associated with geothermal power generation as well as environmental prevention and remediation measures connected to ore mining and milling, but also rare earth element hydrometallurgy, and recycling.

Acknowledgements

We thank Dr. Robert Möckel from TU Bergakademie Freiberg for XFA measurements and Sabrina Beutner for ICP-MS analysis.

Funding

This work was funded by the German Federal Ministry of Economic Affairs and Energy BMWi (SMILE project with grant 02E 11668B).

References

Anand, R.R., Gilkes, R.J., 1987. Muscovite in Darling Range bauxitic laterite. Soil Res. 25, 445–450.

Arnold, T., Utsunomiya, S., Geipel, G., Ewing, R.C., Baumann, N., Brendler, V., 2006. Adsorbed U(VI) surface species on muscovite identified by laser fluorescence spectroscopy and transmission electron microscopy. Environ. Sci. Technol. 40, 4646–

Arnold, T., Zorn, T., Zänker, H., Bernhard, G., Nitsche, H., 2001. Sorption behavior of U(VI) on phyllite: Experiments and modeling. J. Contam. Hydrol. 47, 219–231.

BGE, 2020. Bundesgesellschaft für Endlagerung. Zwischenbericht Teilgebiete gemäß § 13 StandAG 1–444, Berlin, Stand September 2020.

Blanc, P., Vieillard, P., Gailhanou, H., Gaboreau, S., Marty, N., Claret, F., Madé, B., Giffaut, E., 2015. ThermoChimie database developments in the framework of cement/clay interactions. Appl. Geochemistry 55, 95–107.

Blyth, A.R., Frape, S.K., Tullborg, E.-L., 2009. A review and comparison of fracture mineral investigations and their application to radioactive waste disposal. Appl. Geochemistry 24, 821–835. https://doi.org/10.1016/j.apgeochem.2008.12.036

Britz, S., 2018. 'Europium sorption experiments with muscovite, orthoclase, and quartz: Modeling of surface complexation and reactive transport.' PhD Thesis. Technical University Carolo-Wilhelmina Brunswick. Brunswick, Germany.

Bulai, P., Balan, C., Scripcariu, C., Macoveanu, M., 2009. Equilibrium and kinetic studies of copper (II) removal on purolite S930 resin. Environ. Eng. Manag. J. 8, 1103–1109. https://doi.org/10.30638/eemj.2009.161

Charlton, S.R., Parkhurst, D.L., 2011. Modules based on the geochemical model PHREEQC for use in scripting and programming languages. Comput. Geosci. 37, 1653–1663. https://doi.org/10.1016/j.cageo.2011.02.005

Dada, A.O., Olalekan, A.P., Olatunya, A.M., Dada, O., 2012. Langmuir, Freundlich, Temkin and Dubinin–Radushkevich Isotherms Studies of Equilibrium Sorption of Zn 2+ Unto Phosphoric Acid Modified Rice Husk. IOSR J. Appl. Chem. 3, 38–45. https://doi.org/10.9790/5736-0313845

Davies, C.W., Association, I., 1962. Butterworths: Washington. DC, USA 41.

Degueldre, C., Baeyens, B., Goerlich, W., Riga, J., Verbist, J., Stadelmann, P., 1989. Colloids in water from a subsurface fracture in granitic rock, Grimsel Test Site, Switzerland. Geochim. Cosmochim. Acta 53, 603–610. https://doi.org/10.1016/0016-7037(89)90003-3

Demnitz, M., Molodtsov, K., Schymura, S., Schierz, A., Müller, K., Jankovsky, F., Havlova, V., Stumpf, T., Schmidt, M., 2022. Effects of surface roughness and mineralogy on the sorption of Cm(III) on crystalline rock. J. Hazard. Mater. 423, 127006. https://doi.org/10.1016/j.jhazmat.2021.127006

Dzombak, D.A., Morel, F.M.M., 1990. Surface complexation modeling: hydrous ferric oxide. John Wiley & Sons.

Edelstein, N., Klenze, R., Fanghänel, T., Hubert, S., 2006. Optical properties of Cm(III) in crystals and solutions and their application to Cm(III) speciation. Coord. Chem. Rev. 250, 948–973. https://doi.org/10.1016/j.ccr.2006.02.004

Eibl, M., Virtanen, S., Pischel, F., Bok, F., Lönnrot, S., Shaw, S., Huittinen, N., 2019. A spectroscopic study of trivalent cation (Cm3+ and Eu3+) sorption on monoclinic zirconia (ZrO_2). Appl. Surf. Sci. 487, 1316–1328. https://doi.org/10.1016/j.apsusc.2019.05.012

García, D., Lützenkirchen, J., Petrov, V., Siebentritt, M., Schild, D., Lefèvre, G., Rabung, T., Altmaier, M., Kalmykov, S., Duro, L., Geckeis, H., 2019. Sorption of Eu(III) on quartz at high salt concentrations. Colloids Surfaces A Physicochem. Eng. Asp. 578, 123610. https://doi.org/10.1016/j.colsurfa.2019.123610

Geckeis, H., Schäfer, T., Hauser, W., Rabung, T., Missana, T., Degueldre, C., Möri, A., Eikenberg, J., Fierz, T., Alexander, W.R., 2004. Results of the colloid and radionuclide retention experiment (CRR) at the Grimsel Test Site (GTS), Switzerland - Impact of reaction kinetics and speciation on radionuclide migration. Radiochim. Acta 92, 765–774. https://doi.org/10.1524/ract.92.9.765.54973

Giffaut, E., Grivé, M., Blanc, P., Vieillard, P., Colàs, E., Gailhanou, H., Gaboreau, S., Marty, N., Madé, B., Duro, L., 2014. Andra thermodynamic database for performance assessment: ThermoChimie. Appl. Geochemistry 49, 225–236. https://doi.org/10.1016/j.apgeochem.2014.05.007

Grawunder, A., Merten, D., Büchel, G., 2014. Origin of middle rare earth element enrichment in acid mine drainage-impacted areas. Environ. Sci. Pollut. Res. 21, 6812–6823. https://doi.org/10.1007/s11356-013-2107-x

643 Grivé, M., Duro, L., Colàs, E., Giffaut, E., 2015. Thermodynamic data selection applied to
644 radionuclides and chemotoxic elements: An overview of the ThermoChimie-TDB. Appl.
645 Geochemistry 55, 85–94. https://doi.org/10.1016/j.apgeochem.2014.12.017
646 Hao, X., Wang, D., Wang, P., Wang, Y., Zhou, D., 2016. Evaluation of water quality in
647 surface water and shallow groundwater: a case study of a rare earth mining area in southern
648 Jiangxi Province, China. Environ. Monit. Assess. 188, 1–11. https://doi.org/10.1007/s10661-
649 015-5025-1
650 Hartmann, E., Baeyens, B., Bradbury, M.H., Geckeis, H., Stumpf, T., 2008. A Spectroscopic
651 Characterization and Quantification of M(III)/Clay Mineral Outer-Sphere Complexes.
652 Environ. Sci. Technol. 42, 7601–7606. https://doi.org/10.1021/es801092f
653 Hartmann, E., Brendebach, B., Polly, R., Geckeis, H., Stumpf, T., 2011. Characterization and
654 quantification of Sm(III)/ and Cm(III)/clay mineral outer-sphere species by TRLFS in D_2O
655 and EXAFS studies. J. Colloid Interface Sci. 353, 562–568.
656 https://doi.org/10.1016/j.jcis.2010.09.067
657 Hayes, K.F., Redden, G., Ela, W., Leckie, J.O., 1991. Surface complexation models: An
658 evaluation of model parameter estimation using FITEQL and oxide mineral titration data. J.
659 Colloid Interface Sci. 142, 448–469. https://doi.org/10.1016/0021-9797(91)90075-J
660 Ho, Y.S., Porter, J.F., Mckay, G., 2002. Divalent Metal Ions Onto Peat : Copper , Nickel and
661 Lead Single Component Systems. Water, Air, Soil Pollut. 141, 1–33.
662 Huittinen, N., Rabung, T., Andrieux, P., Lehto, J., Geckeis, H., 2010. A comparative batch
663 sorption and time-resolved laser fluorescence spectroscopy study on the sorption of Eu(III)
664 and Cm(III) on synthetic and natural kaolinite. Radiochim. Acta 98, 613–620.
665 https://doi.org/10.1524/ract.2010.1761
666 Huittinen, N., Rabung, T., Lützenkirchen, J., Mitchell, S.C., Bickmore, B.R., Lehto, J.,
667 Geckeis, H., 2009. Sorption of Cm(III) and Gd(III) onto gibbsite, α-$Al(OH)_3$: A batch and
668 TRLFS study. J. Colloid Interface Sci. 332, 158–164.
669 https://doi.org/10.1016/j.jcis.2008.12.017
670 Huittinen, N., Rabung, T., Schnurr, A., Hakanen, M., Lehto, J., Geckeis, H., 2012. New
671 insight into Cm(III) interaction with kaolinite – Influence of mineral dissolution. Geochim.
672 Cosmochim. Acta 99, 100–109. https://doi.org/10.1016/j.gca.2012.09.032
673 Jackson, M.L., Tyler, S.A., Willis, A.L., Bourbeau, G.A., Pennington, R.P., 1948. Weathering
674 sequence of clay-size minerals in soils and sediments. I: Fundamental generalizations. J.
675 Phys. Colloid Chem. 52, 1237–1260. https://doi.org/10.1021/j150463a015

676 Keesmann, S., Noseck, U., Buhmann, D., Fein, E., Schneider, A., 2005. Modellrechnungen
677 zur Langzeitsicherheit von Endlagern in Salz-und Granitformationen. Gesellschaft für
678 Anlagen- und Reaktorsicherheit (GRS) gGmbH. Braunschweig, Germany, Report 206.
679 Kim, J.I., Klenze, R., Wimmer, H., Runde, W., Hauser, W., 1994. A study of the carbonate
680 complexation of CmIII and EuIII by time-resolved laser fluorescence spectroscopy. J. Alloys
681 Compd. 213–214, 333–340. https://doi.org/10.1016/0925-8388(94)90925-3
682 Kimura, T., Choppin, G.R., Kato, Y., Yoshida, Z., 1996. Determination of the Hydration
683 Number of Cm(III) in Various Aqueous Solutions. Radiochim. Acta 72, 61–64.
684 Kupcik, T., Rabung, T., Lützenkirchen, J., Finck, N., Geckeis, H., Fanghänel, T., 2016.
685 Macroscopic and spectroscopic investigations on Eu(III) and Cm(III) sorption onto bayerite
686 (β-$Al(OH)_3$) and corundum (α-Al_2O_3). J. Colloid Interface Sci. 461, 215–224.
687 https://doi.org/10.1016/j.jcis.2015.09.020
688 Laverov, N.P., Yudintsev, S. V., Kochkin, B.T., Malkovsky, V.I., 2016. The Russian strategy
689 of using crystalline rock as a repository for nuclear waste. Elements 12, 253–256.
690 https://doi.org/10.2113/gselements.12.4.253
691 Lee, S.-G., Lee, K.Y., Cho, S.Y., Yoon, Y.Y., Kim, Y., 2006. Sorption properties of 152Eu
692 and 241Am in geological materials: Eu as an analogue for monitoring the Am behaviour in
693 heterogeneous geological environments. Geosci. J. 10, 103–114.
694 https://doi.org/10.1007/BF02910354
695 Lee, S.S., Schmidt, M., Laanait, N., Sturchio, N.C., Fenter, P., 2013. Investigation of
696 structure, adsorption free energy, and overcharging behavior of trivalent yttrium adsorbed at
697 the muscovite (001)-water interface. J. Phys. Chem. C 117, 23738–23749.
698 https://doi.org/10.1021/jp407693x
699 Lützenkirchen, J., Behra, P., 1996. On the surface precipitation model for cation sorption at
700 the (hydr)oxide water interface. Aquat. Geochemistry 1, 375–397.
701 https://doi.org/10.1007/BF00702740
702 Marques Fernandes, M., Stumpf, T., Baeyens, B., Walther, C., Bradbury, M.H., 2010.
703 Spectroscopic identification of ternary Cm - Carbonate surface complexes. Environ. Sci.
704 Technol. 44, 921–927. https://doi.org/10.1021/es902175w
705 Merten, D., Geletneky, J., Bergmann, H., Haferburg, G., Kothe, E., Büchel, G., 2005. Rare
706 earth element patterns: A tool for understanding processes in remediation of acid mine
707 drainage. Chemie der Erde 65, 97–114. https://doi.org/10.1016/j.chemer.2005.06.002

Molodtsov, K., Demnitz, M., Schymura, S., Jankovský, F., Zuna, M., Havlová, V., Schmidt, M., 2021. Molecular-Level Speciation of Eu(III) Adsorbed on a Migmatized Gneiss As Determined Using μ-TRLFS. Environ. Sci. Technol. 55, 4871–4879. https://doi.org/10.1021/acs.est.0c07998

Molodtsov, K., Schymura, S., Rothe, J., Dardenne, K., Schmidt, M., 2019. Sorption of Eu(III) on Eibenstock granite studied by μ-TRLFS: A novel spatially-resolved luminescence-spectroscopic technique. Sci. Rep. 9, 6287. https://doi.org/10.1038/s41598-019-42664-2

Möri, A., Alexander, W.R., Geckeis, H., Hauser, W., Schäfer, T., Eikenberg, J., Fierz, T., Degueldre, C., Missana, T., 2003. The colloid and radionuclide retardation experiment at the Grimsel Test Site: Influence of bentonite colloids on radionuclide migration in a fractured rock. Colloids Surfaces A Physicochem. Eng. Asp. 217, 33–47. https://doi.org/10.1016/S0927-7757(02)00556-3

NEA, 2006. Organisation for Economic Co-operation and Development and Nuclear Energy Agency (OECD-NEA). Physics and Safety of Transmutation Systems. OECD Pap. 6, 1–120.

Neumann, J., Brinkmann, H., Britz, S., Lützenkirchen, J., Bok, F., Stockmann, M., Brendler, V., Stumpf, T., Schmidt, M., 2021. A comprehensive study of the sorption mechanism and thermodynamics of f-element sorption onto K-feldspar. J. Colloid Interface Sci. 591, 490–499. https://doi.org/10.1016/j.jcis.2020.11.041

Neumann, J., Lee, S.S., Brinkmann, H., Eng, P.J., Stubbs, J.E., Stumpf, T., Schmidt, M., 2022. Impact of Ion-Ion Correlations on the Adsorption of M(III) (M = Am, Eu, Y) onto Muscovite (001) in the Presence of Sulfate. J. Phys. Chem. C 126, 1400–1410. https://doi.org/10.1021/acs.jpcc.1c09561

Neumann, J, Qiu, C., Eng, P., Skanthakumar, S., Soderholm, L., Stumpf, T., Schmidt, M., 2021. Effect of Background Electrolyte Composition on the Interfacial Formation of Th(IV) Nanoparticles on the Muscovite (001) Basal Plane. J. Phys. Chem. C 125, 16524–16535. https://doi.org/10.1021/acs.jpcc.1c03997

Ojovan, M.I., Lee, W.E., Kalmykov, S.N., 2019. An introduction to nuclear waste immobilisation, 3rd Edition. Elsevier.

Oy, P., 2012. Posiva, Olkiluoto site description Report 2011. Eurajoki, Finland. ISSN 1239-3096

Pan, D., Fan, F., Wang, Y., Li, P., Hu, P., Fan, Q., Wu, W., 2017. Retention of Eu(III) in muscovite environment: Batch and spectroscopic studies. Chem. Eng. J. https://doi.org/10.1016/j.cej.2017.07.184

741 Parkhurst, D.L., Appelo, C.A.J., 2013. Description of input and .examples for PHREEQC
742 version 3: a computer program for speciation, batch-reaction, one-dimensional transport, and
743 inverse geochemical calculations, Techniques and Methods. Reston, VA.
744 https://doi.org/10.3133/tm6A43
745 Poeter, E.P., Hill, M.C., Lu, D., Tiedeman, C., Mehl, S.W., 2014. UCODE_2014, with new
746 capabilities to define parameters unique to predictions, calculate w eights using simulated
747 values, estimate parameters with SVD, evaluate uncertainty with MCMC, and more.
748 Rabung, T., Geckeis, H., Wang, X.K., Rothe, J., Denecke, M.A., Klenze, R., Fanghänel, T.,
749 2006. Cm(III) sorption onto γ-Al2O3: New insight into sorption mechanisms by time-
750 resolved laser fluorescence spectroscopy and extended X-ray absorption fine structure.
751 Radiochim. Acta 94, 609–618. https://doi.org/10.1524/ract.2006.94.9-11.609
752 Richter, C., 2015. Sorption of environmentally relevant radionuclides (U(VI), Np(V)) and
753 lanthanides (Nd(III)) on feldspar and mica. PhD Thesis. Technical University Dresden.
754 Dresden, Germany.
755 Richter, C., Müller, K., Drobot, B., Steudtner, R., Großmann, K., Stockmann, M., Brendler,
756 V., 2016. Macroscopic and spectroscopic characterization of uranium(VI) sorption onto
757 orthoclase and muscovite and the influence of competing Ca2+. Geochim. Cosmochim. Acta
758 189, 143–157. https://doi.org/10.1016/j.gca.2016.05.045
759 Schnurr, A., Marsac, R., Rabung, T., Lützenkirchen, J., Geckeis, H., 2015. Sorption of
760 Cm(III) and Eu(III) onto clay minerals under saline conditions: Batch adsorption, laser-
761 fluorescence spectroscopy and modeling. Geochim. Cosmochim. Acta 151, 192–202.
762 https://doi.org/10.1016/j.gca.2014.11.011
763 Soler, J.M., Mäder, U.K., 2010. Cement-rock interaction: Infiltration of a high-pH solution
764 into a fractured granite core. Geol. Acta 8, 221–233. https://doi.org/10.1344/105.000001531
765 Stockmann, M., Schikora, J., Becker, D.A., Flügge, J., Noseck, U., Brendler, V., 2017. Smart
766 Kd-values, their uncertainties and sensitivities - Applying a new approach for realistic
767 distribution coefficients in geochemical modeling of complex systems. Chemosphere 187,
768 277–285. https://doi.org/10.1016/j.chemosphere.2017.08.115
769 Stumpf, S., Stumpf, T., Dardenne, K., Hennig, C., Foerstendorf, H., Klenze, R., Fanghänel,
770 T., 2006a. Sorption of Am(III) onto 6-Line-Ferrihydrite and Its Alteration Products:
771 Investigations by EXAFS. Environ. Sci. Technol. 40, 3522–3528.
772 https://doi.org/10.1021/es052518e

Stumpf, S., Stumpf, T., Walther, C., Bosbach, D., Fanghänel, T., 2006b. Sorption of Cm(III) onto different Feldspar surfaces: a TRLFS study. Radiochim. Acta 94, 243–248. https://doi.org/10.1524/ract.2006.94.5.243

Stumpf, T., Hennig, C., Bauer, A., Denecke, M.A., Fanghänel, T., 2004. An EXAFS and TRLFS study of the sorption of trivalent actinides onto smectite and kaolinite. Radiochim. Acta 92, 133–138. https://doi.org/10.1524/ract.92.3.133.30487

Stumpf, T., Rabung, T., Klenze, R., Geckeis, H., Kim, J.I., 2001. Spectroscopic study of Cm(III) sorption onto γ-alumina. J. Colloid Interface Sci. 238, 219–224. https://doi.org/10.1006/jcis.2001.7490

Vokál, A., Vopálka, D., Večerník, P., 2010. An approach for acquiring data for description of diffusion in safety assessment of radioactive waste repositories. J. Radioanal. Nucl. Chem. 286, 751–757. https://doi.org/10.1007/s10967-010-0763-6

Wang, Z., Giammar, D.E., 2013. Mass Action Expressions for Bidentate Adsorption in Surface Complexation Modeling: Theory and Practice. Environ. Sci. Technol. 47, 3982–3996. https://doi.org/10.1021/es305180e

Wilson, M.J., 2004. Weathering of the primary rock-forming minerals: processes, products and rates. Clay Miner. 39, 233–266. https://doi.org/10.1180/0009855043930133

Yamamoto, K., Yoshida, H., Akagawa, F., Nishimoto, S., Metcalfe, R., 2013. Redox front penetration in the fractured Toki Granite, central Japan: An analogue for redox reactions and redox buffering in fractured crystalline host rocks for repositories of long-lived radioactive waste. Appl. Geochemistry 35, 75–87. https://doi.org/10.1016/j.apgeochem.2013.03.013

Yan, L., Masliyah, J.H., Xu, Z., 2013. Interaction of divalent cations with basal planes and edge surfaces of phyllosilicate minerals: Muscovite and talc. J. Colloid Interface Sci. 404, 183–191. https://doi.org/10.1016/j.jcis.2013.04.023

Zhao, P., Begg, J.D., Zavarin, M., Tumey, S.J., Williams, R., Dai, Z.R., Kips, R., Kersting, A.B., 2016. Plutonium(IV) and (V) Sorption to Goethite at Sub-Femtomolar to Micromolar Concentrations: Redox Transformations and Surface Precipitation. Environ. Sci. Technol. 50, 6948–6956. https://doi.org/10.1021/acs.est.6b00605